MHD rotating flow over a stretching surface: The role of viscosity and aggregation of nanoparticles

Aisha M. Alqahtani [a], Khadija Rafique [b,*], Zafar Mahmood [b], Bushra R. Al-Sinan [c], Umar Khan [b], Ahmed M. Hassan [d]

[a] *Department of mathematical sciences, College of Science, Princess Nourah bint Abdulrahman University, P. O. Box 84428, Riyadh 11671, Saudi Arabia*
[b] *Department of Mathematics and Statistics, Hazara University, Mansehra, Pakistan*
[c] *Department of Administrative and Financial Sciences, Nairiyah College, University of Hafr Al-Batin, Hafr Al-Batin 31991, Saudi Arabia*
[d] *Center of Research, Faculty of Engineering, Future University in Egypt, New Cairo, 11835, Egypt*

ABSTRACT

The magnetohydrodynamic (MHD) rotating flow that occurs across a stretching surface has numerous practical applications in a variety of domains. These fields include astronomy, engineering, the material sciences, and space exploration. The combined examination of magneto-hydrodynamics rotating flow across a stretching surface, taking into consideration fluctuating viscosity and nanoparticle aggregation, has significant ramifications across several different domains. It is essential for both the growth of technology and the attainment of deeper insights into the complicated fluid dynamics to maintain research in this field. Given the aforementioned motivation, the principal aim of this study is to examine the effects of variable viscosity on the bidirectional rotating magnetohydrodynamic flow over a stretching surface. Aggregation effects on nanoparticles are used in the analysis. Titania (TiO_2) is taken nanoparticle and ethylene glycol as base fluid. The nonlinear ordinary differential equations and the boundary conditions that correspond to them can be transformed into a dimensionless form by using a technique called similarity transformation. To get a numerical solution to the transformed equation, the Runge-Kutta 4th order (RK-4) method is utilized, and this is done in conjunction with the shooting method. The impact of various leading variables on dimensionless velocity, the coefficients of temperature, skin friction and local Nusselt number are graphically represented. Velocity profiles in both direction increases with increasing values of φ. The Nusselt number increases with increasing values of the radiation and temperature ratio parameters. When a 1 % volume fraction of nanoparticles is introduced, the Nusselt number exhibits a 0.174 % increase for the aggregation model compared to the regular fluid in the absence of radiation effects. When the aggregation model is used with a 1 % volume fraction of nanoparticles, the skin friction increases by 0.1153 % in the x direction and by 0.1165 % in the y direction compared to the regular fluid. Tables show the variation in Nusselt numbers, as well as a comparison of the effects of nanoparticle's aggregation model without and with radiation. Moreover, the numerical results obtained were compared with previously published data, demonstrating a satisfactory agreement. We firmly believe that this finding will have extensive implications for engineering and various industries.

* Corresponding author.
E-mail address: khadijarafique101@gmail.com (K. Rafique).

1. Introduction

Nanofluids have recently attracted a lot of attention in engineering and industrial applications, principally because they are able to improve heat transfer procedures. As a means of improving thermal efficiency, nanoparticles of metals such as aluminium, gold, copper, and iron, as well as the oxides of these elements, are frequently used as additives. In most cases, these metal nanoparticles are mixed with widely used base fluids such as water, glycol, or ethylene. These nanofluids have attracted a lot of attention and are currently serving as the impetus for the development of an entirely new category of heat transfer fluids. Jana and his colleagues [1] did an important study in which they found that nanofluids with metal nanoparticles had a significant rise in their thermal conductivity. As Choi [2] demonstrates, the addition of nanoparticles results in an increase in the thermal conductivity of the fluid that is equivalent to approximately twice its previous value. Experiments of Xuan and Li [3] have shown that thermal conductivity of the suspensions increasing 20 % more due to small concentration of nanoparticle. Akbarinia et al. [4] studied that nanofluids have a lower viscosity are more stable and have better properties on hard surfaces. Gold, cooper silver alumni and their oxides are the most used nanoparticles, while oil, water, ethylene, and glycol are the most frequently used base fluids. Nanofluids find extensive and diverse practical applications, including cooling, air conditioning mobile phones, computer processors, and many others. Many researchers have extensively investigated the mathematical and experimental properties of nanofluids. Chamkha et al. [5] investigated in depth an important application of nanofluid in micro channel.

The analysis of both fluid flows that obey or do not obey Newton law of viscosity has many engineering and industrial applications over a stretched surface, including wire drawing, paper and glass fiber production, crystal growing, and many others. Several studies on stretching surface flows have resulted in a lot of attention over the last two centuries. Thermal diffusion effects of convicted fluid on a stretched surface were investigated by Patil et al. [6]. They modeled the problem by integrating the impacts of the thermal diffusion time and the magnetic field. Later, in Ref. [7] they studied mixed convection over decreasing flow velocity. Zeeshan et al. [8] numerically studied coupled stress fluid over an inclined plane in the occurrence of metallic nanoparticles. However, researchers are now paying more attention to stretching. Seth and Mishra [9] have recently studied the Navier slip condition and effects of thermal radiation on flow of nanofluids boundary layer while keeping in mind the non-linearity of the stretching rates. Many other researchers studied different flow scenarios with different condition over stretched surfaces in Refs. [10–13].

Abd El-Aziz [14] investigate how radiation affects flow of fluid on a moving surface. Mukhopadyay [15] investigated effects of thermal radiation in problem of heat transfer by mixed convection of the unstable boundary layer from vertical stretched surface submerged in a porous medium. Shateyi and Motsa [16] have newly numerically investigated the transfer of heat and mass in a fluid on a horizontal stretched sheet. The study undertaken by Ganie et al. [17] investigated the impact of non-linear thermal radiation on a stretching surface, utilising the Yamada-Ota model.

Magnetohydrodynamics is study of movement of electrically conductive fluids in presence of magnetic field. Engineers applied magnetohydrodynamics concept to the design of many industrial applications including; Propulsion, nuclear waste disposal, heat exchanger generators, magnetohydrodynamics pumps, geothermal energy extractors and nuclear reactor cooling (Yashkun et al. [18]), Devi and Devi [19] numerically studied regular flow on MHD hybrid nanofluids in two dimension through a stretch plate with suction. They discovered that by increasing the magnetic field strength temperature of hybrid nanofluids increased while the velocity decreased. Devi and Devi [19] did his work in Devi and Devi [20] for regular flow in three dimensions. The effect of magnetic field strength was same on velocity and temperature in a three dimension of constant flux. Ali et al. [21] conducted a study to find out how nanoparticle aggregation affects the flow of magnetohydrodynamic (MHD) nanofluids along a thin needle-like structure. Waini et al. [22] studied heat transfer in flow of stable hybrid nanofluids in a two-dimensional exponential stretch/shrink layer.

The rotational flow is used in rotating machinery, medical instruments, power generation systems, electronic devices, air purification devices, computer storage equipment, gas turbine rotors and other applications. Transfer of heat has been studied by Hayat and Nadeem [23] using stable hybrid nanofluid of $Ag - CuO/$water rotational flow in three dimension. Adnan Asghar and Teh Yuan Ying [24] studied a magnetohydrodynamic hybrid nanofluid in three dimension over a rotating stretch/shrink sheet. They also studied the joule heating effect. The concentration profile grew as rotation parameter was increased. Patil et al. [25,26] examined the impact of impulsive motion and mixed convection on the fluid flow around a rotating sphere.

Numerous studies have been done to demonstrate the aggregation of nanoparticles (NP) into nanofluids [27–30]. He et al. [31] discovered that NP aggregation has an impact on heat transfer in a titanium nanofluid heat transfer study. When NP aggregation occurred, the viscosity increased. Ellahi et al. [32] refer to NP aggregates the same as the chains when mixture of alumina and water flows over nanofluid wedge. Mackolil and Mahanthesh [33] have used aggregation of the titania nano liquid with based ethylene glycol to calculate the heat transfer in the convective flow of marangoni. It was deliberate, the thermophysical properties changed when NP aggregate. Makhdoum et al. [34] recently conducted extensive research on nanoparticle aggregation and entropy generation of nanofluids over stretching sheet. Using the theory of Brownian motion and the diffusion-limited aggregation model, Xuan et al. [35] were able to show how nanoparticles move randomly and how they join together to form larger structures. Mahmood and khan [36] studied effects of nanoparticles aggregation on unstable flow of stagnation point of hydrogen oxide-based nanofluids. Researchers looked at the effect that heat transfer and nanoparticle aggregation had on the mixed convective stagnation point flow across a Riga plate in Ref. [37].

The fluid properties are known to change with temperature investigated by Eringen [38]. The rise in temperature causes rise in transport phenomena due to decreasing viscosity through a momentum boundary layer, which affects heat transfer rate by side of wall. The impact of viscosity which is varying and thermal conductivity on magnetohydrodynamic flow and heat transfer on a stretch sheet was investigated by Salem [39]. The impact of viscosity which is varying and thermal conductivity of an unstable laminar flow of

incompressible viscous conductive fluid in two dimension passing in front of a vertical porous moving plate having variable suction was studied by Seddeek and Salama [40]. The changes of properties with respect to temperature have many applications in chemical engineering. Mukhopadhyay et al. [41] studied MHD boundary layer flow having variable viscosity over heated stretched sheet. Recently researchers have studied flow and heat transfer on stretched surface in various flow scenarios with variable viscosity in Refs. [42–44].

MHD rotational flow across a rotating surface has a variety of applications, including material coating, thin film technology, bioengineering, and energy conversion, to name a few. It is possible to significantly improve heat and mass transfer rates in industrial processes by making use of the surface stretching technique. The application of a magnetic field and the introduction of rotational motion both have the advantage of further optimizing the effectiveness of the procedure. Using a rotating flow of magnetohydro-dynamic (MHD) fluid over a stretched surface makes it easier to deposit thin films with exact thickness and uniformity. The field of thin film technology is where this application truly shines regarding its significance. The use of a stretching surface provides a regulated method to govern the process of film deposition, while the concurrent application of both a magnetic field and rotational motion contributes to the achievement of the desired qualities and characteristics of the thin films. The MHD rotating flow across a stretching surface offers a wide variety of fascinating applications, all of which consider the impact that viscosity and nanoparticle aggregation have on the flow. These applications investigate a wide variety of possibilities and situations that can arise within the context of magnetohydrodynamics and nanotechnology. The deposition of nanoparticles onto a substrate in a manner that is both accurate and under control is an example of one application of this type of technology. The flow behavior, which governs the transport and dispersion of nanoparticles within the fluid medium, is substantially impacted by the viscosity of the fluid. The existence of viscosity is a critical factor in determining the appearance of these phenomena and the way they interact with one another inside the flow. In addition, nanoparticle aggregation, which is driven by factors such as the attraction between van Der Waals particles, is an additional essential factor that influences the overall process. When it comes to controlling the deposition process and achieving the desired nanoparticle patterns and coatings, the interaction between viscosity, aggregation, and MHD flow is of the utmost importance. This newfound knowledge has a great deal of potential to produce nanoparticles. The introduction of precursor solutions that are loaded with nanoparticles into the flow that is taking place across the stretching surface promotes increased mixing and reaction rates, which makes the synthesis process much simpler. Viscosity has a significant impact on the flow behavior as well as the interaction that occurs between the precursor solutions; on the other hand, nanoparticle aggregation can influence the size as well as the properties of the synthesized nanoparticles. It has been brought to the author's knowledge that the investigation of an MHD ternary hybrid nanofluid across a stretching surface, considering the effects of changing viscosity and nanoparticle aggregation, has not yet been undertaken. As a result, the focus of this ongoing research has shifted to an investigation of this field. In this paper, we investigate the effect that varying viscosity has on the bidirectional rotating flow of MHD across a stretched surface, additionally, the influence of nanoparticle aggregation on the flow. The nonlinear ordinary differential equations and their accompanying coupled boundary conditions can be transformed into a dimensionless form by applying the similarity transformation method. This allows the equations to be solved in a more straightforward manner. Subsequently, the equations, transformed through similarity transformation, are numerically solved using the RK4 method combined with the shooting method. The graphical depiction presents an illustration of the impacts that various fundamental parameters have on dimensionless coefficients such as temperature and velocity. Both tables and graphs are used to show how the values of the local coefficients of skin friction and the local Nusselt number are affected by the relevant parameters. The analysis demonstrates that the physical parameters have a significant impact on the fluid flow.

2. Description of the problem

The regular incompressible laminar flow in three dimension a bidirectional impermeable stretching surface will be considered with linear velocities $u = ax$ and $v = by$, where a and b are taken as constants. Cartesian coordinate is chosen such a way that the surface is associated with the $xy-$ plane and fluid is considered in the $z \geq 0$ space titania (TiO_2) nanoparticle with ethylene glycol $(C_2H_6O_2)$ are used as base fluid. Here vicious dissipation is neglected. The Newtonian material is electrically conducting through the application of constant magnetic force along z–axis. The magneto Reynolds number is presumed to be smaller, and due to this assumption; the induced-magnetized field is ignored. The fluid rotation is about the $z-$ axis. The constant surface temperature T_w and ambient temperature T_∞ are assumed.

The thermophysical characteristics of both the base fluid and the nanoparticles are outlined in Table 1. Except for the viscosity of the base fluid, which is inversely dependent on temperature, the thermophysical properties of the ambient fluids are assumed to remain constant. To study the variable viscosity and thermal conductivity of nanofluids, modified aggregation models will be used in this study. Taking these assumptions and the typical boundary layer approximation into account, the governing equations for the problem, which include the laws of conservation of mass, momentum, and energy and account for the fact that the viscosity of the fluid

Table 1
The nanoparticles' thermophysical characteristics with base fluid (see Ref. [36]).

Properties	TiO_2	$C_2H_6O_2$
$\rho \ (kg\ /m3)$	4250	1114
$Cp \ (J\ /kgK)$	686.2	2415
$\sigma(\Omega m)^{-1}$	2.38×10^6	1.07×10^{-6}
$k \ (W\ /mK)$	8.9538	0.252

can change, are as follows: (See Refs. [24,36]):

$$\frac{\partial u}{\partial x} + \frac{\partial v}{\partial y} + \frac{\partial w}{\partial z} = 0,\tag{1}$$

$$u\frac{\partial u}{\partial x} + v\frac{\partial u}{\partial y} + w\frac{\partial u}{\partial z} - 2\Omega v = \frac{1}{\rho_{nf}}\frac{\partial}{\partial z}\left(\mu_{nf}\frac{\partial u}{\partial z^2}\right) - \frac{\sigma_{nf}}{\rho_{nf}}B_0^2 u,\tag{2}$$

$$u\frac{\partial v}{\partial x} + v\frac{\partial v}{\partial y} + w\frac{\partial v}{\partial z} + 2\Omega u = \frac{1}{\rho_{nf}}\frac{\partial}{\partial z}\left(\mu_{nf}\frac{\partial v}{\partial z^2}\right) - \frac{\sigma_{nf}}{\rho_{nf}}B_0^2 v,\tag{3}$$

$$u\frac{\partial T}{\partial x} + v\frac{\partial T}{\partial y} + w\frac{\partial T}{\partial z} = \frac{k_{nf}}{(\rho C_p)_{nf}}\frac{\partial^2 T}{\partial z^2} - \frac{1}{(\rho C_p)_{nf}}\left(\frac{\partial q_r}{\partial z}\right).\tag{4}$$

u, v and w represent the velocity component along three axes: x, y and z. The radiative heat flux q_r is taken according to the Roseland approximation as (see Ref. [36]):

$$q_r = -\frac{16\sigma^* T^3}{3k^*}\frac{\partial T}{\partial z},\tag{5}$$

Here, k^* is average absorption coefficient, σ^* is the Stephen-Boltzmann constant. By putting equation (5) in equation (4) energy equation becomes:

$$u\frac{\partial T}{\partial x} + v\frac{\partial T}{\partial y} + w\frac{\partial T}{\partial z} = \frac{k_{nf}}{(\rho C_p)_{nf}}\frac{\partial^2 T}{\partial z^2} + \frac{1}{(\rho C_p)_{nf}}\frac{16\sigma^*}{3k^*}\frac{\partial}{\partial z}\left(T^3\frac{\partial T}{\partial z}\right).\tag{6}$$

Next, the boundary conditions are: see (see Ref. [24])

$$\left.\begin{array}{l} u = ax, v = \alpha by, w = 0, T = T_w \text{ at } z = 0, \\ u\to 0, v\to 0, T\to T_\infty \text{ as } z\to\infty. \end{array}\right]\tag{7}$$

Nanofluid temperature is T, μ_{nf} is dynamic viscosity, ρ_{nf} is density, thermal conductivity is k_{nf} and heat capacity $(\rho C_p)_{nf}$. The thermophysical properties are selected based on the NP's aggregation property. To calculate the effective variable viscosity and thermal conductivity when there is no aggregation present, the modified Brinkman and Maxwell models are used. The effective properties of the nanoliquids are summarized in Table 2.

During the computation of these equations, several variables need to be considered. φ, represents the solid volume part of nanofluid, where the effective nanofluid is characterized by dynamic viscosity denoted as μ_{nf} and μ_f signifies the viscosity coefficient, which is assumed to vary inversely with temperature according to the following relationship (see Refs. [42–44]):

$$\frac{1}{\mu_f} = \frac{1}{\mu_{f_\infty}}[1 + \delta(T - T_\infty)] \text{ i.e., } \frac{1}{\mu_f} = a(T - T_r),\tag{8}$$

Here,

$$a = \frac{\delta}{\mu_{f_\infty}}, T_r = T_\infty - \frac{1}{\delta}$$

The selection of reference temperatures for the sake of correlations turns out to be quite practical for most applications. In this case, the thermal characteristics of the fluid and the reference position δ (which is a constant) determine the values of the constants a and T_r

Table 2
Models of nanoliquid with effective thermophysical properties (see Ref. [36]).

Effective Property	Without Aggregation	With Aggregation
Density	$\frac{\rho_{nf}}{\rho_f} = (1 - \varphi) + \varphi\frac{\rho_S}{\rho_f}$	$\frac{\rho_{nf}}{\rho_f} = (1 - \varphi_a) + \varphi_a\frac{\rho_S}{\rho_f}$
Dynamic Viscosity	$\mu_{nf} = \frac{\mu_f}{(1 - \varphi)^{2.5}}$	$\mu_{nf} = \mu_f\left(1 - \frac{\varphi_a}{\varphi_m}\right)^{-[\eta]\varphi_m}$
Specific Heat Capacity	$\frac{(\rho C_p)_{nf}}{(\rho C_p)_f} = (1 - \varphi) + \varphi\frac{(\rho C_p)_S}{(\rho C_p)_f}$	$\frac{(\rho C_p)_{nf}}{(\rho C_p)_f} = (1 - \varphi_a) + \varphi_a\frac{(\rho C_p)_S}{(\rho C_p)_f}$
Thermal Conductivity	$\frac{k_{nf}}{k_f} = \frac{(k_S + 2k_f) - 2\varphi(k_f - k_S)}{(k_S + 2k_f) + \varphi(k_f - k_S)}$	$\frac{k_{nf}}{k_f} = \frac{(k_a + 2k_f) - 2\varphi_a(k_f - k_a)}{(k_a + 2k_f) + \varphi_a(k_f - k_a)}$
Electrical Conductivity	$\frac{\sigma_{nf}}{\sigma_f} = 1 + \frac{3\left(\frac{\sigma_s}{\sigma_f} - 1\right)\varphi}{\left(\frac{\sigma_s}{\sigma_f} + 2\right) - \left(\frac{\sigma_s}{\sigma_f} - 1\right)\varphi}$	$\frac{\sigma_{nf}}{\sigma_f} = 1 + \frac{3\left(\frac{\sigma_s}{\sigma_f} - 1\right)\varphi_a}{\left(\frac{\sigma_s}{\sigma_f} + 2\right) - \left(\frac{\sigma_s}{\sigma_f} - 1\right)\varphi_a}$

respectively. In the case of liquids, $a > 0$ whereas in the case of gases, $a < 0$. T stands for the temperature, while T_∞ and μ_{f_∞} denote constant values of the viscosity coefficient and temperature, respectively, at a distance that is very far away from the surface.

The nanofluid density is ρ_{nf}, while the base fluid density is ρ_f. Nanofluids have k_{nf} thermal conductivity and $((\rho C_p)_{nf})$ heat capacity. Base fluid heat conductivity is k_f.

The Krieger-Dougherty model was modified to account for nanoparticle aggregation, as shown in Table 2. According to experimental studies (see, e.g., in Ref. [36]), then nanoparticle aggregation is a key factor in dynamics and flows of nanofluid. When aggregation component was taken into relation, nanomaterial measured outcomes agreed exactly. Aggregation kinetic factor, effects nanoparticle volume fraction and it becomes $\left(\varphi_a = \varphi \left(\frac{r_a}{r_p} \right)^{3-D} \right)$. In terms of spherical and dispersion-limited aggregation, $D = 1.8, \frac{r_a}{r_p} = 3.34, \varphi_m = 0.605$ and $[\eta] = 2.5$). The aggregation model used for thermal conductivity was developed by combining the Brugman model with the Maxwell model, which was later modified. Thermal conductivity of the aggregate (k_a) (see Ref. [36]), can be determined by using the following formula:

$$\frac{k_a}{k_f} = \frac{1}{4} \left\{ (3\varphi_{in} - 1)\frac{k_S}{k_f} + (3(1 - \varphi_{in}) - 1) + \left[\left((3\varphi_{in} - 1)\frac{k_S}{k_f} + (3(1 - \varphi_{in}) - 1) \right)^2 + 8\frac{k_S}{k_f} \right]^{\frac{1}{2}} \right\}. \text{ Here, } \varphi_{in} = \left(\frac{r_a}{r_p} \right)^{D-3}.$$

The insertion of dimensionless velocities, temperature, and the variable η as:

$$u = axf^{'}(\eta), v = byg^{'}(\eta), w = -\sqrt{a\upsilon}(f + g), T = T_\infty[1 + (\theta_w - 1)\theta(\eta)], \theta_w = \frac{T_w}{T_\infty}, \eta = \sqrt{\frac{a}{\upsilon}}z. \tag{9}$$

Where the prime notation indicates differentiation with respect to η. Considering Eq. (9), Eqs. (1)–(3) and (6) and (7) are reduced to the following boundary value problem:

$$\frac{f^{'''}}{1 - \frac{\theta}{\theta_r}} + \frac{f^{''}\theta^{'}}{\theta_r \left(1 - \frac{\theta}{\theta_r} \right)^2} = -A_1 A_2 \left[(f + g)f^{''} - f^{'2} + 2\lambda g^{'} - \frac{B_1}{A_2} Mf^{'} \right], \tag{10}$$

$$\frac{g^{'''}}{1 - \frac{\theta}{\theta_r}} + \frac{g^{''}\theta^{'}}{\theta_r \left(1 - \frac{\theta}{\theta_r} \right)^2} = -A_1 A_2 \left[(f + g)g^{''} - g^{'2} - 2\lambda f^{'} - \frac{B_1}{A_2} Mg^{'} \right], \tag{11}$$

$$\left((A_3 + Rd(1 + (\theta_w - 1)\theta)^3)\theta^{'} \right)^{'} + \Pr A_4 (f + g)\theta^{'} = 0, \tag{12}$$

Here

$A_1 = (1 - \varphi)^{2.5},$ (For without aggregation model) &

$A_1 = \left(1 - \frac{\varphi_a}{\varphi_m} \right)^{-[\eta]\varphi_m},$ (For with aggregation model)

$A_2 = (1 - \varphi) + \varphi\frac{\rho_S}{\rho_f},$ (For without aggregation model) &

$A_2 = (1 - \varphi_a) + \varphi_a\frac{\rho_S}{\rho_f},$ (For with aggregation model)

$A_3 = \frac{(k_S + 2k_f) - 2\varphi(k_f - k_S)}{(k_S + 2k_f) + \varphi(k_f - k_S)}$ (For without aggregation model) &

$A_3 = \frac{(k_a + 2k_f) - 2\varphi_a(k_f - k_a)}{(k_a + 2k_f) + \varphi_a(k_f - k_a)}$ (For aggregation model)

$$A_4 = (1 - \varphi) + \varphi \frac{(\rho C_p)_S}{(\rho C_p)_f} \text{ (For without aggregation}$$
$$\text{model) \&}$$

$$A_4 = (1 - \varphi_a) + \varphi_a \frac{(\rho C_p)_S}{(\rho C_p)_f} \text{ (For with aggregation}$$
$$\text{model)}$$

$$B_1 = 1 + \frac{3\left(\frac{\sigma_s}{\sigma_f} - 1\right)\varphi}{\left(\frac{\sigma_s}{\sigma_f} + 2\right) - \left(\frac{\sigma_s}{\sigma_f} - 1\right)\varphi} \text{ (For without aggregation}$$
$$\text{model) \&}$$

$$B_1 = 1 + \frac{3\left(\frac{\sigma_s}{\sigma_f} - 1\right)\varphi_a}{\left(\frac{\sigma_s}{\sigma_f} + 2\right) - \left(\frac{\sigma_s}{\sigma_f} - 1\right)\varphi_a} \text{ (For with aggregation}$$
$$\text{model).}$$

Boundary conditions transformation (7) into

$$f(0) = g(0) = 0, f'(0) = 1, g'(0) = \alpha, \theta(0) = 1,$$

$$f'(\eta) \to 0, g'(\eta) \to 0, \theta(\eta) \to 0, \text{ as } \eta \to \infty. \tag{13}$$

In the previous equations, $\lambda = \frac{\Omega}{a}$ denotes a rotation parameter, $Pr = \frac{(\rho C_p)_f}{k_f}$ shows the Prandtl number. By $\alpha = \frac{b}{a}$, we are referring to the stretch or shrink parameter, here $\alpha > 0$ indicates a stretching sheet and $\alpha < 0$ represents a shrinking sheet. $Rd = \frac{4\sigma^* T_\infty^3}{3kk^*}$ denote the radiation parameter. $\theta_w = \frac{T_f}{T_\infty}$ is temperature ratio parameter. $\theta_r = -1/[\delta(T_w - T_\infty)]$ is fluid viscosity. $M = \frac{\sigma_f B_0^2}{\rho_f a}$ is magnetic parameter. The investigation primarily focuses on the friction coefficients Cf_x and Cf_y along x axes, y axes as well as the local Nusselt number Nu_x. These factors hold significant importance in the study.

$$C_{fx} = \frac{\tau_{\tilde{w}x}}{\rho_f u_w^2}, C_{fy} = \frac{\tau_{\tilde{w}y}}{\rho_f v_w^2}, N\tilde{u}_x = \frac{xq_{\tilde{w}}}{k_f(T_w - T_\infty)}. \tag{14}$$

The symbols $\tau_{\tilde{w}x}$, $\tau_{\tilde{w}y}$ represent the shear stresses along the x and y axes, respectively, while $q_{\tilde{w}}$ symbolizes the heat flux. These terms are provided below:

$$\tau_{\tilde{w}x} = \mu_{nf}\left(\frac{\partial u}{\partial z}\right)_{z=0}, \tau_{\tilde{w}y} = \mu_{nf}\left(\frac{\partial v}{\partial z}\right)_{z=0}, q_{\tilde{w}} = -k_{nf}\left[\left(\frac{\partial T}{\partial z}\right)_{z=0} + (q_r)_{z=0}\right]. \tag{15}$$

Upon invoking equations (9), (14 and 15), we obtain the following results (see Ref. [24]):

$$Re_x^{1/2} C_{fx} = \frac{1}{A_1\left(1 - \frac{\theta}{\theta_r}\right)} f''(0), Re_y^{1/2} C_{fy} = \frac{1}{A_1\left(1 - \frac{\theta}{\theta_r}\right)} g''(0),$$

$$Re_x^{-1/2} Nu_x = -\left[\left(A_3 + Rd(1 + (\theta_w - 1)\theta)^3\right)\theta'(0)\right]\theta'(0), \tag{16}$$

where $Re_x = \frac{\tilde{a}x^2}{v_f}$ and $Re_y = \frac{(\tilde{b})y^2}{v_f}$ represent the local Reynolds numbers along x and $y-$ axes, respectively.

3. Solution methodology

The coupled ordinary differential equations 10–12 as well as the boundary conditions (13) that are linked with them are extremely complex and nonlinear in their character. It is advised that a numerical scheme be used to solve these equations, particularly for the purpose of capturing the various physical factors that are present in the flow routes of nanofluid. To accomplish this, we will use a strategy that combines the Runge-Kutta (RK) method and the shooting method. The sequence in which the same momentum and energy equations 10 and 11 are utilized determines the transformations that must take place to start the process, as well as the boundary domains that are specified in equation (13). As a result of these modifications, the complex model is transformed into an initial value problem, which can be easily solved as follows:

$$\Xi_1 = f, \Xi_2 = f', \Xi_3 = f'', \Upsilon_1 = g, \Upsilon_2 = g', \Upsilon_3 = g'', \Lambda_1 = \theta, \Lambda_2 = \theta', \tag{17}$$

using equation (17),

$$\Xi_1' = f', \Xi_2' = f'', \Xi_3' = f''', \Upsilon_1' = g', \Upsilon_2' = g'', \Upsilon_3' = g''', \Lambda_1' = \theta', \Lambda_2' = \theta'', \tag{18}$$

The following findings are a direct consequence of solving equations (17) and (18).

$$\Xi_1' = \Xi_2, \Xi_2' = \Xi_3, \Xi_3' = f''', \Upsilon_1' = \Upsilon_2, \Upsilon_2' = \Upsilon_3, \Upsilon_3' = g''', \Lambda_1' = \Lambda_2, \Lambda_2' = \theta'', \tag{19}$$

By arranging equations 10–12 as bellow, we will obtain the values of f''', g''' and θ'' that appear in equation (19):

$$f''' = -\left(1 - \frac{\theta}{\theta_r}\right)\left[\frac{f''\theta'}{\theta_r\left(1 - \frac{\theta}{\theta_r}\right)^2} + A_1 A_2\left[(f+g)f'' - f'^2 + 2\lambda g' - \frac{B_1}{A_2}Mf'\right]\right], \tag{20}$$

$$g''' = -\left(1 - \frac{\theta}{\theta_r}\right)\left[\frac{g''\theta'}{\theta_r\left(1 - \frac{\theta}{\theta_r}\right)^2} + A_1 A_2\left[(f+g)g'' - g'^2 - 2\lambda f' - \frac{B_1}{A_2}Mg'\right]\right], \tag{21}$$

$$\theta'' = -\frac{\Pr A_4(f+g)\theta'}{\left((A_3 + Rd(1 + (\theta_w - 1)\theta)^3)\right)}. \tag{22}$$

It is important to incorporate the values from equations (17) and (19) into equations (20) and (21) correspondingly to solve the initial value problem. For obtaining numerical solutions for equations 20–22, the robust computational software package known as Mathematica 10 is used. One of its distinctive features is its ability to classify the main system of equations and apply the most suitable numerical method to provide an accurate solution to the problem. Because most numerical methods are impractical for handling semi-infinite situations, the infinite norm is substituted with a suitable finite value of η, This is done because most numerical methods are unworkable. Despite this modification, there are no discernible shifts in the physical phenomena that are associated with the system.

4. Results and discussion

This part highlights a few remarkable results. To study the flow behavior relevant physical parameters are presented by graphs and numerically. Fig. 1 shows a physical model of flow of particle aggregation nanofluids. Fig. 2 depicts a model simulation flow chart. Figs. 3–27 depict behavior of velocity, behavior of temperature, behavior of skin friction, and Nusselt number profiles, that's provide an overall picture of the present situation. The value of the Prandtl number $Pr = 6.96$ remains constant at 6.96 throughout this study, except when comparing it with previous cases. In the tables and figures, it is evident that the control parameter values are varied dynamically. The selection of these numbers is based on how effectively they satisfy the far-field boundary conditions. The volume fraction of nanofluid is selected within range of $0.01 \leq \varphi \leq 0.04$. Other parameters are chosen based on main references and possibility of solutions in stretching flow. This means that $0.1 \leq \lambda \leq 1.0$ (rotation parameter), $0.1 \leq M \leq 0.5$ (magnetic parameter), $0.2 \leq Rd \leq$
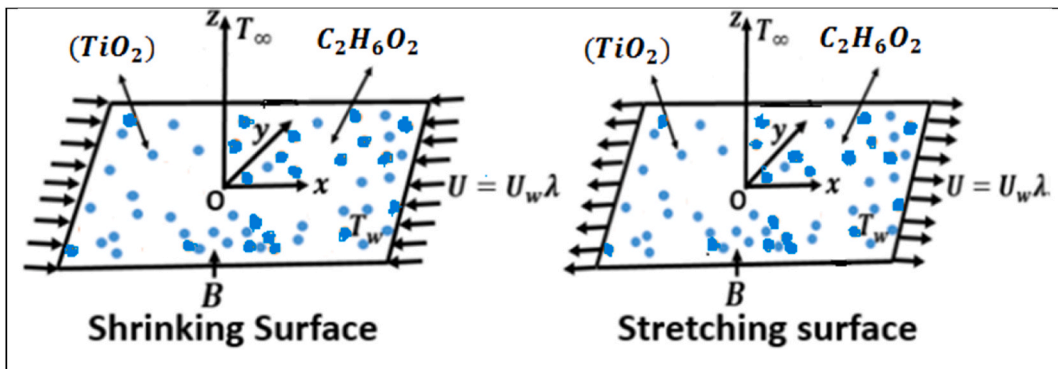
Fig. 1. Physical model diagram.
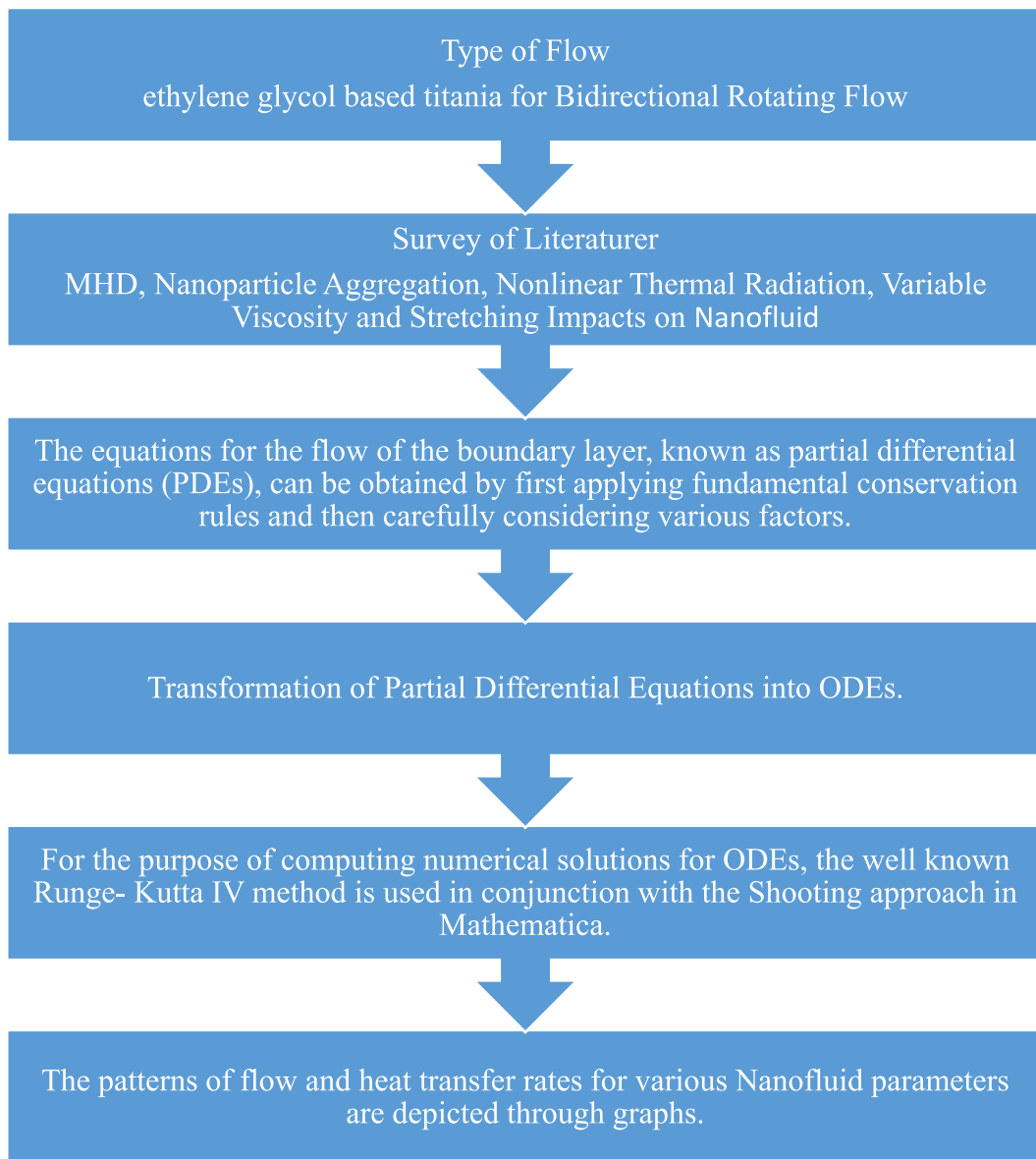
Fig. 2. Mathematical demonstration of the problem.

1.0 (thermal radiation parameter), $0.005 \leq \alpha \leq 0.02$ (stretching parameter), $-2.5 \leq \theta_r \leq -0.5$ (viscosity parameter), $0.05 \leq \theta_w \leq 0.3$ (temperature ratio parameter). These values are used if the distant-field limit criteria are met. In the following sub-section (4.1–4.3) outlines that how the velocity and temperature profiles are determined by numerous regulating factors as well as coefficients in engineering are examined particularly. The investigation is concluded in two modes (1) with aggregation $\varphi_a \neq 1$, and (2) without aggregation for $TiO_2 - C_2H_6O_2$ nanofluid on bidirectional rotating flow over a stretching surface.

4.1. Velocity profile $f'(\eta)$ and $g'(\eta)$

This sub-section discusses the effects of effective parameters like nanoparticle volume fraction φ, fluid viscosity θ_r, magnetic M, rotation λ and stretching α on the fluid velocity in both directions $f'(\eta)$ and $g'(\eta)$. The graphs are sketched for two scenarios: with and without aggregation. The behavior of the parameters is identical in both cases, except for numerical variations. Effect of M and φ on the velocities along $x-$ axis $f'(\eta)$ and $y-$ axis $g'(\eta)$ are presented in Figs. 3–6 respectively. When the aggregation effect is under consideration then in this case speed profiles are lower. Therefore, as expected, due to the nanoparticle's aggregation, the speed of the fluid decreases. From Figs. 3 and 4, due to increase in M both $f'(\eta)$ and $g'(\eta)$ decreases. The magnetic field can induce Lorentz forces in the fluid, which act perpendicular to both the magnetic field and the fluid flow direction. These forces can oppose and slow down the fluid
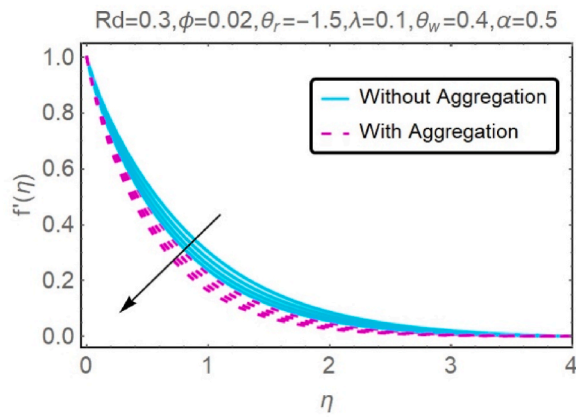
Fig. 3. Velocity profile $f'(\eta)$ against $M = 0.1, 0.2, 0.3, 0.4$.
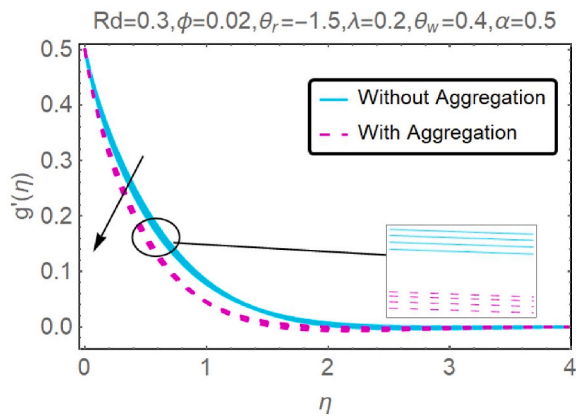
Fig. 4. Velocity profile $g'(\eta)$ against $M = 0.1, 0.2, 0.3, 0.4$.
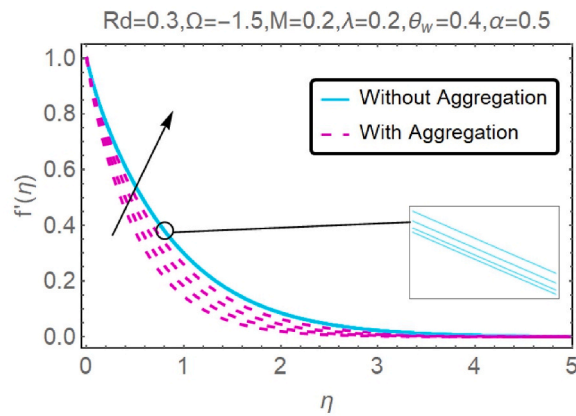
Fig. 5. Velocity profile $f'(\eta)$ against $\varphi = 0.01, 0.02, 0.03, 0.04$.

flow, leading to a decrease in the velocity profile. In MHD rotating flows, the impact of magnetic parameters becomes pronounced, and the fluids rotational motion can be affected, resulting in a reduction in the overall velocity in both aggregation and without aggregation case. Physically, it is the outcome of Lorentz force which is caused due to increase in M. The effects of φ on $f'(\eta)$ and $g'(\eta)$ are sketched in Figs. 5 and 6. The double nature is seen when decrease in $f'(\eta)$ and $g'(\eta)$ till $\eta \approx 1$ after that the increase in φ gives an increase in $f'(\eta)$ and $g'(\eta)$. The volume fraction is a measure of the nanoparticles' concentration in a nanofluid. This can also be written as the volume
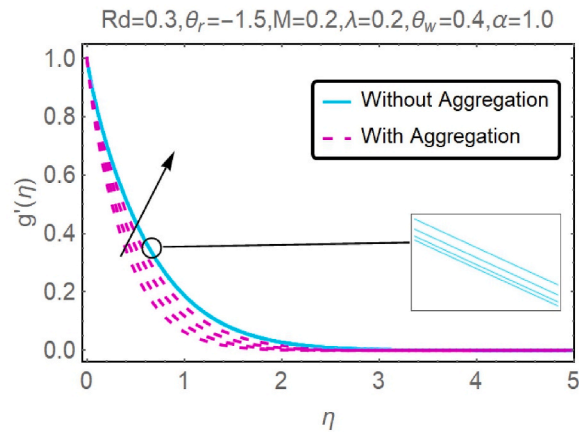
Fig. 6. Velocity profile $g'(\eta)$ against $\varphi = 0.01, 0.02, 0.03, 0.04$.
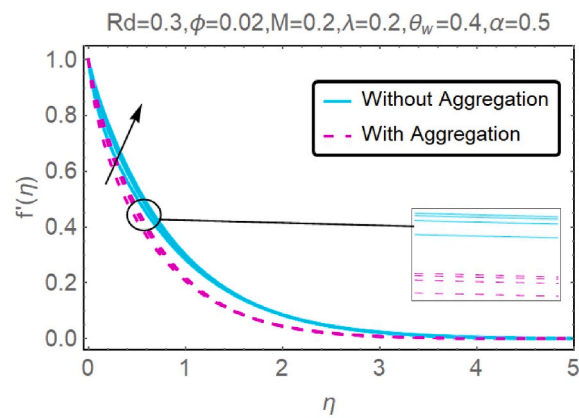
Fig. 7. Velocity profile $f'(\eta)$ against $\theta_r = -0.5, -1.0, -1.5, -2.0$.
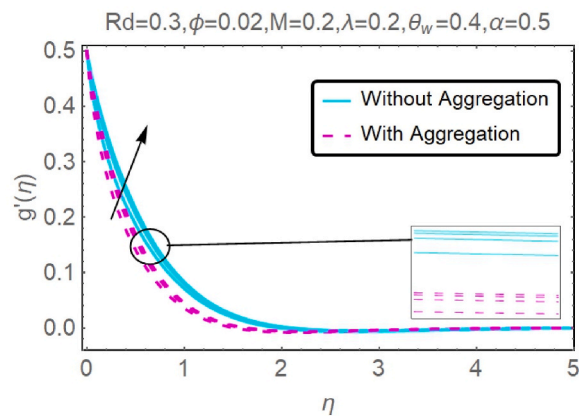
Fig. 8. Velocity profile $g'(\eta)$ against $\theta_r = -0.5, -1.0, -1.5, -2.0$.

fraction ratio. The concentration of nanoparticles in the nanofluid rises in tandem with the increasing volume percentage of the nanofluid. In most cases, the thermal conductivity of nanoparticles is significantly higher than that of the basic fluid. This increase in thermal conductivity can result in increased heat transfer rates, particularly in the presence of a stretching surface, which can contribute to the rise in velocity profile. This is one of the factors that can contribute to the rise in velocity profiles.

Variable viscosity parameter effect on nondimensional velocities profiles in both directions are represented in Figs. 7 and 8. When
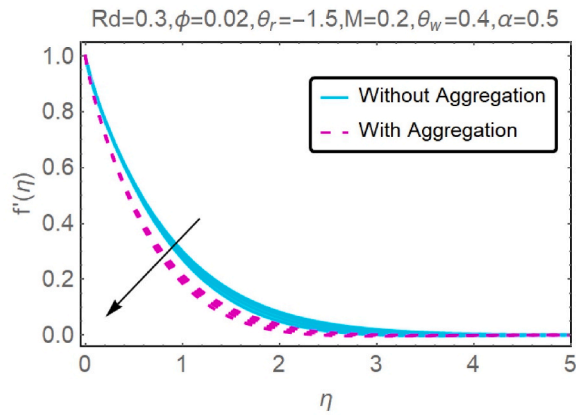
Fig. 9. Velocity profile $f'(\eta)$ against $\lambda = 0.2, 0.3, 0.4, 0.5$.
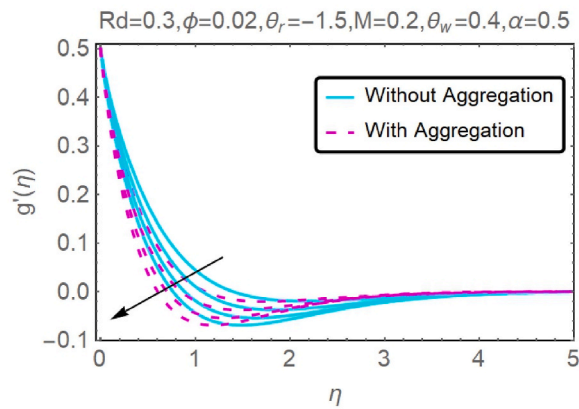
Fig. 10. Velocity profile $g'(\eta)$ against $\lambda = 0.2, 0.3, 0.4, 0.5$.
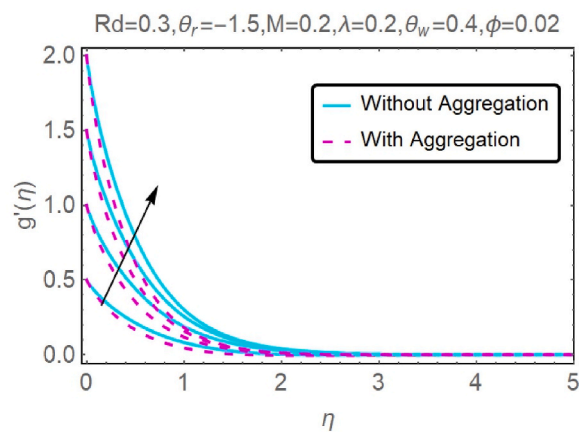
Fig. 11. Velocity profile $g'(\eta)$ against $\alpha = 0.2, 0.4, 0.6, 0.8..$

$\theta_r \rightarrow 0$ the boundary layer thickness decreased. When values of Prandtl number are greater than velocity distribution becomes linear. Indeed, for a fluid which is given, when δ fixed, lower θ_r implies greater difference in temperature among ambient fluid and wall. The results depicted in this article reveal clearly θ_r, which is a sign of the changes in the viscosity of the fluid w. r.t temperature, has strong impact on velocity profile $f'(\eta)$ and $g'(\eta)$ with the boundary layer therefore on friction characteristics of skin. The viscosity parameter is what defines the amount of viscous force and represents the fluid's internal resistance to flow. When the viscosity parameter is
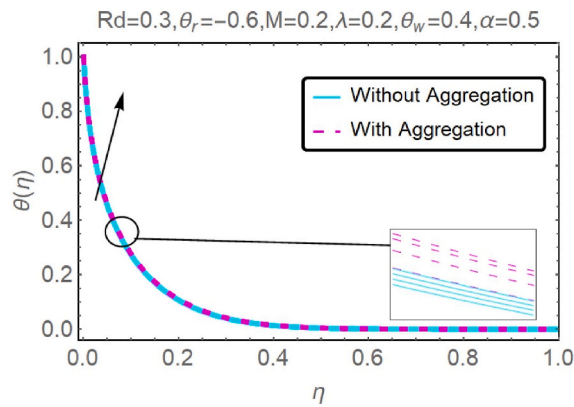
Fig. 12. Profile of temperature θ(η) vs $\varphi = 0.01, 0.02, 0.03, 0.04$.
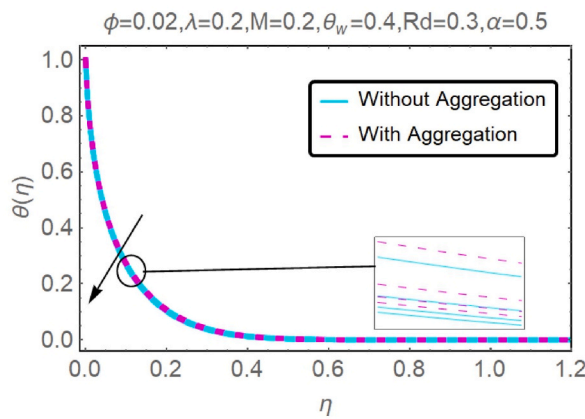
Fig. 13. Profile of temperature θ(η) vs $\theta_r = -0.5, -1.0, -1.5, -2.0$.
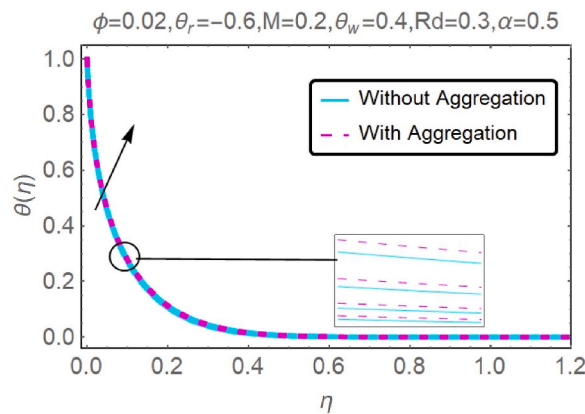
Fig. 14. Profile of temperature θ(η) vs $\lambda = 0.1, 0.3, 0.5, 0.7$.

lowered, the internal friction that occurs within the fluid will also be lowered. As a result of this, the fluid encounters a lower level of viscous resistance when it is stretched against the surface, which enables it to flow more easily. A higher velocity profile results from this decrease in viscous resistance, which causes the viscosity to decrease. If the viscosity parameter is decreased, then the fluid particles that are closer to the surface will typically suffer reduced stickiness or adhesion to the solid border. Therefore, the slip velocity at the surface increases because of this. The slip velocity refers to the relative velocity between the fluid and the solid surface, and when this velocity increases, it enhances the overall velocity profile.
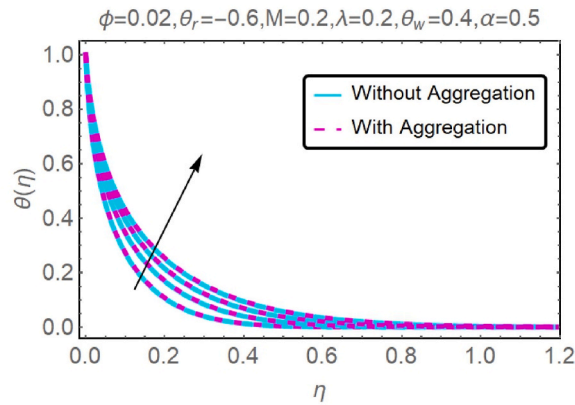
Fig. 15. Profile of temperature θ(η) vs $Rd = 0.2, 0.4, 0.6, 0.8$.
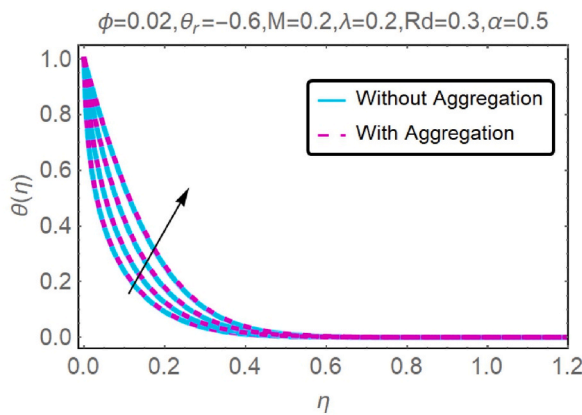
Fig. 16. Profile of temperature θ(η) vs $\theta_w = 0.2, 0.4, 0.6, 0.8$.
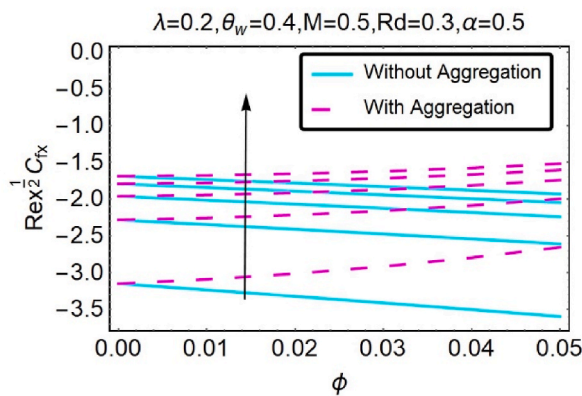
Fig. 17. Skin friction of $\theta_r = -0.5, -1.0, -1.5, -2.0, -2.5$ against φ.

The influence of rotation parameter λ on speed profile $f'(\eta)$ and $g'(\eta)$ profiles are exhibited in Figs. 9 and 10. In Figs. 9 and 10, when value of the parameter of rotation λ increases, both fluid velocities $f'(\eta)$ and $g'(\eta)$ are decreases. The rotation parameter stands for the angular velocity of the surface that is being stretched. If you have a higher value for the rotation parameter, the stretching surface will revolve at a faster rate. As a consequence of this, there is an increase in centrifugal force that acts on fluid particles that are close to surface. Because of this centrifugal force, the fluid tends to be pushed away from the surface, which results in a decrease in the velocity profile as well as a reduction in the velocity near the surface. This shows that thickness of momentum decreases for increasing values of
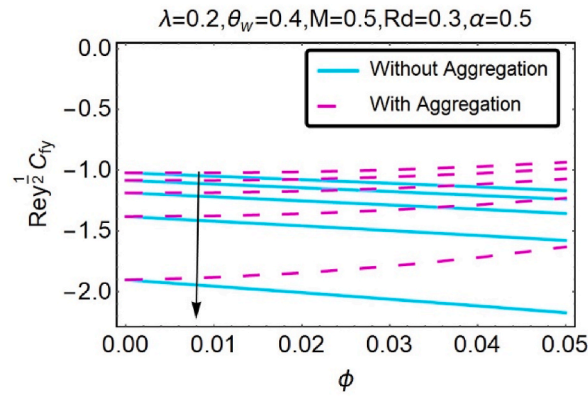
Fig. 18. Skin friction of $\theta_r = -0.5, -1.0, -1.5, -2.0, -2.5$ against φ.
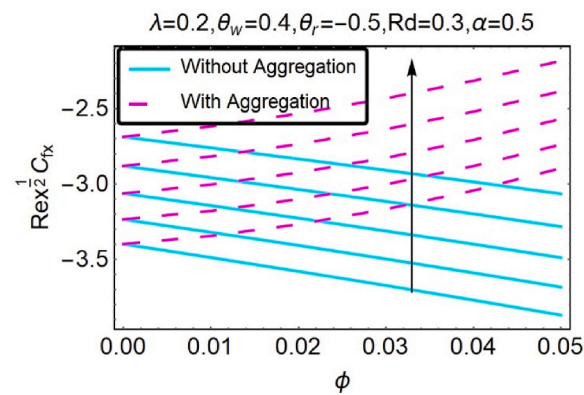
Fig. 19. Skin friction of $M = 0.1, 0.2, 0.3, 0.4, 0.5$ against φ.
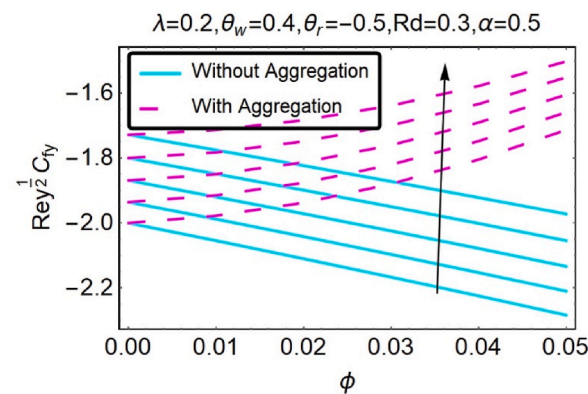
Fig. 20. Skin friction of $M = 0.1, 0.2, 0.3, 0.4, 0.5$ against φ.

λ. Fig. 11 shows impression of a stretching parameter α on the velocity profiles $g'(\eta)$ of the $TiO_2 - C_2H_6O_2$ nanofluid flow. We can say that the increasing value of α causes velocity field to increase. When the surface is stretched more quickly, a greater volume of nanofluid will flow across it. This is because the surface is being stretched. A greater stretching parameter results in an increased flow rate, which in turn translates to higher velocities throughout the flow field. This is because the flow rate is directly proportional to the volume of fluid that is moving through a given region in a given amount of time.
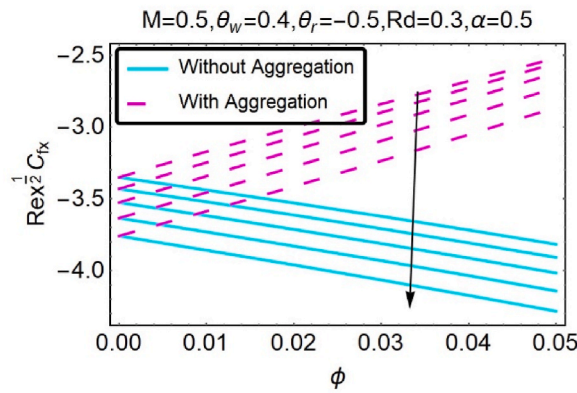
Fig. 21. Skin friction of $\lambda = 0.2, 0.4, 0.6, 0.8, 1.0$ against φ.
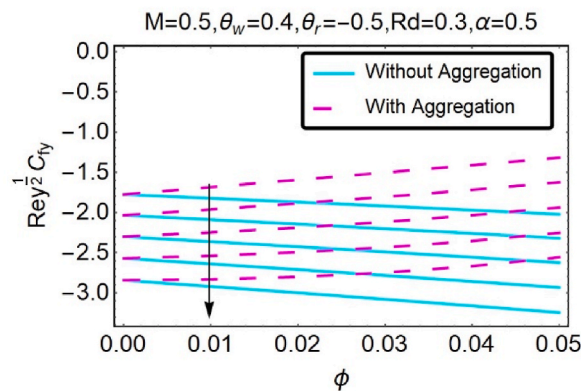
Fig. 22. Skin friction of $\lambda = 0.2, 0.4, 0.6, 0.8, 1.0$ against φ.
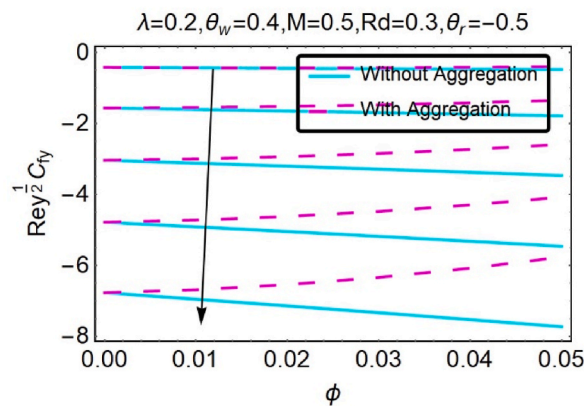
Fig. 23. Skin friction of $\alpha = 0.2, 0.4, 0.6, 0.8, 1.0$ against φ.

4.2. Temperature profile $\theta(\eta)$

This sub-section discusses the effect of several physical parameters on dimensionless temperature profile $\theta(\eta)$. In Fig. 12, $\theta(\eta)$ rises due to increase in φ. It is due to the increment in thermal conductivity of nanoliquid due to increase in φ. It is very interesting that due to increasing values of φ the case when aggregation is taking place, temperature profiles increase higher than the case when it is neglected. The formation of a nanofluid requires the addition of nanoparticles to a base fluid. The presence of these nanoparticles can greatly increase thermal conductivity of fluid. In most cases, thermal conductivity of nanoparticles is significantly higher than that of
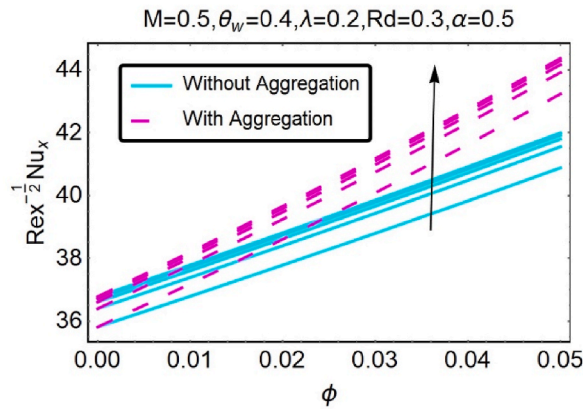
Fig. 24. Nusselt number $\theta_r = -0.5, -1.0, -1.5, -2.0, -2.5$ against φ.
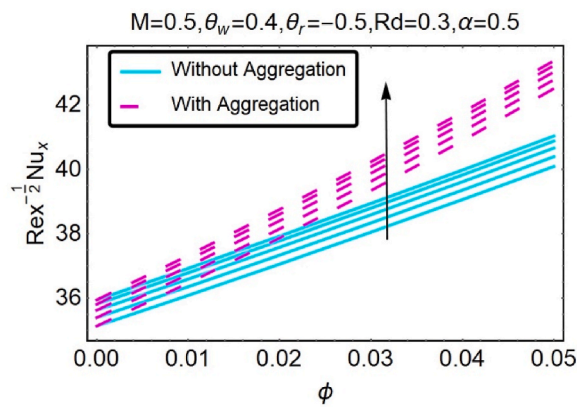
Fig. 25. Nusselt number $\lambda = 0.2, 0.4, 0.6, 0.8, 1.0$ against φ.
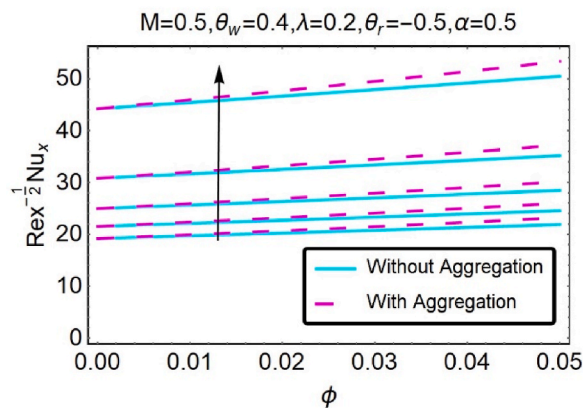
Fig. 26. Nusselt number $Rd = 0.2, 0.4, 0.6, 0.8, 1.0$ against φ.

base fluid. Increment in the volume fraction parameter result in increases in the concentration of nanoparticles present in the nanofluid, which in turn leads to improvements in the nanofluid's capacity to transmit heat. As a result of this, heat is more efficiently transferred from the stretched surface to the surrounding fluid, leading to an overall increase in the temperature profile. The impact of variable viscosity parameter θ_r against temperature profile is presented in Fig. 13 for both cases (without aggregation and with aggregation). A graphical representation shows that the lower viscosity parameter of the fluid θ_r has effect of reducing the temperature. This is because of fact that the decrease in viscosity parameter of fluid θ_r reduces thermal boundary layer thickness, that's lead to a
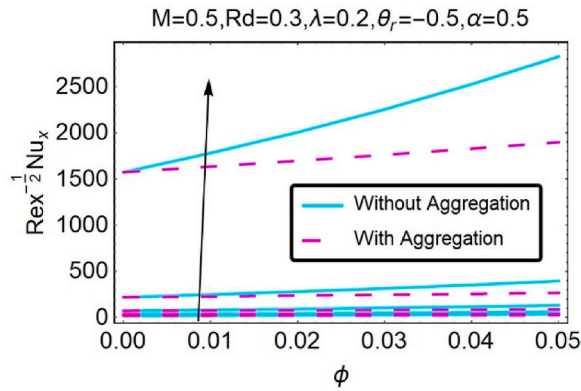
Fig. 27. Nusselt number $\theta_w = 0.1, 0.3, 0.5, 0.7, 0.9$ against φ.

decrease in temperature. The viscosity parameter stands for the internal resistance that the nanofluid offers to the flow of fluid. When the viscosity parameter is lowered, both the amount of internal friction and the amount of energy that is lost within the fluid are lowered as well. Because of this decrease in viscous dissipation, less energy is turned into heat as a result of the friction that occurs inside the fluid, which ultimately results in lower temperatures within the nanofluid.

Fig. 14 shows effects of rotational parameter λ on temperature profile $\theta(\eta)$. In Fig. 14, when the value of rotational parameter λ increases, fluid temperature increased. This suggests that as the values of λ increase for both aggregation and non-aggregation solutions, the thickness of the thermal boundary layer also increases. The stretching surface rotates at a quicker rate in response to an increase in the rotation parameter. This results in an increase in the centrifugal forces that are acting on the nanofluid. Centrifugal force is a factor in the conversion of kinetic energy into thermal energy, which raises temperature. The centrifugal force may be to blame for this heating. Figs. 15 and 16 disclosed the responses of $\theta(\eta)$ for Rd and θ_w. The influence of Rd on $\theta(\eta)$ is presented in Fig. 15. With rise in Rd, temperature of zone of nanofluid boundary layer increases. This is observed in Fig. 15 that $\theta(\eta)$ is increased by an increased in Rd. An increased in the parameter Rd leads to discharge of thermal energy in direction of flow; therefore fluid $\theta(\eta)$ is increased. The thermal radiation parameter represents the significance of the system's radiative heat transport. When there is an increase in the value of the thermal radiation parameter, there is a corresponding rise in the contribution that radiation makes to the total heat transfer. Thermal radiation can transport heat across surfaces even in the absence of a medium, in contrast to conduction and convection, which require direct contact or the movement of fluids to work. Because of this, an increase in the thermal radiation parameter results in a more effective mechanism for heat transfer, which in turn causes the flow field to experience higher temperatures. It is perceived that for mounting η values of the parameter θ_w, the temperature profile inflates. The rise in temperature profile is caused by increasing parameter θ_w which ultimately results in elevated the temperature of wall as compared to ambient temperature, and fluid temperature enriches. The graphical demonstration shows that $\theta(\eta)$ rise when we increase ratio of force and temperature of thermal radiation. The temperature ratio parameter calculates the percentage difference between the temperatures at the stretched surface and the temperature of the surrounding environment. If the temperature ratio parameter rises, this shows that the fluid around the surface being stretched is at a lower temperature than the surface being stretched itself. Because of this, there is a larger temperature variation between the bulk fluid and the surface of the nanofluid, which causes an increase in the amount of heat that is transferred from the surface to the nanofluid via convection. Temperatures in the nanofluid rise as a consequence of the greater temperature ratio parameter, which boosts the effectiveness of convective heat transfer.

4.3. Heat transfer and skin friction

In this subsection, we will discuss influence of several important physical parameters on engineering coefficients, skin friction and local Nusselt number on both directions is known as rate of heat transfer. Results in numerical form for local skin friction coefficient in term of $Re_x^{1/2}Cf_x$, $Re_y^{1/2}Cf_y$ and local Nusselt number in term of $Re_x^{-1/2}Nu_x$ due to changes in θ_r and φ are shown in Figs. 17, 18 and 24 respectively for stretching sheet. Figure shows that for different values of θ_r, $Re_x^{1/2}Cf_x$, is increasing that means surface have influence on fluid. When the viscosity parameter is lower, the viscous damping, also known as the resistance to flow, is decreased. The viscosity parameter describes the internal friction that exists within the fluid. As a result of this, fluid particles near the surface suffer decreased drag and frictional forces, which leads to an increase in x - direction velocity of fluid. $Re_y^{1/2}Cf_y$ decreases in y-direction for varying values of viscosity. When fluid viscosity is reduced, viscous effects cause the fluid to suffer less heating. There is a reduction in the amount of energy that is lost as heat because of the viscosity; as a direct consequence of this, there is a flatter temperature gradient down the y-axis. Because of this, the buoyancy effects that could potentially drive fluid motion in the y-direction are mitigated, which results in a reduction in surface friction in that direction. Also, θ_r and φ increase, the local Nusselt number increases. It is notice further from Fig. 24 for specific value θ_r the local Nusselt number raised as φ rises from zero to twenty percent. A decrease in viscosity will result in a thinner thermal boundary layer near the surface. The region responsible for transporting heat from the surface to the fluid is

referred to as the thermal boundary layer. A thermal boundary layer that is thinner provides for a more effective transport of heat and a faster dissipation of thermal energy into the fluid, both of which contribute to a greater Nusselt number at the local level.

The impact of M with φ on skin friction in both directions $Re_x^{1/2}Cf_x$, $Re_y^{1/2}Cf_y$ are presented in Figs. 19 and 20. Computations in numerical form suggest that for several values of M solutions exist for both cases of stretching sheet. According to the plotting of $Re_x^{1/2}Cf_x$, $Re_y^{1/2}Cf_y$ explained in Figs. 19 and 20, it is shown that there is an increment in the solution of $Re_x^{1/2}Cf_x$, $Re_y^{1/2}Cf_y$ once M enlarges in the $TiO_2 - C_2H_6O_2$ nanofluid flow. In an electrically conductive fluid presence of magnetic field favors a force, namely Lorentz force. The magnetic parameter gives a representation of the intensity of the magnetic field that is being used. When the value of magnetic parameter rises, the magnetic forces that act upon the nanofluid will exert a greater degree of influence. When it comes to MHD flows, the magnetic field can affect the motion of the fluid and bring about additional viscous effects. These magnetic field-induced viscous effects can lead to increased shear and drag forces near the surface, which ultimately result in higher skin friction in both x and y directions. The synchronization of the magnetic and electric fields resulting from the establishment of resistive force tends to slow down movement of conductive fluid in vicinity of boundary layer. In simple, increase of M increases $Re_x^{1/2}Cf_x$, $Re_y^{1/2}Cf_y$, that results in increment of friction pull exerted on surface of sheet.

The skin friction factors on $Re_x^{1/2}Cf_x$, $Re_y^{1/2}Cf_y$ against φ and for different values of λ is illustrating in Figs. 21 and 22. Skin friction coefficients values $Re_x^{1/2}Cf_x$, $Re_y^{1/2}Cf_y$ are negative thus the fluid will apply a stress on stretched wall (which is the cause of flow). The rotation parameter stands for the angular velocity of the surface that is being stretched. The stretching surface rotates at a quicker rate when the rotation parameter is increased, which causes reduction in the amount of shear that occurs close to the surface. When there is rotation in the flow, the boundary layer tends to become thinner, which lowers the flow resistance at the surface. Because there is less shear at the surface, there is less skin friction in both the x and y directions. Fig. 23 demonstrate the variation of the reduced skin friction $Re_y^{1/2}Cf_y$ in $y-$ direction with respect to φ for the stretching parameter α. From Figure in both shrinking and stretching regions unique solution generally exists for the values of $\alpha > -1$. The domain of the solution has extended to left for each increment in φ. Fig. 23 shows an increment in α with φ decline the value of $Re_y^{1/2}Cf_y$ for both solution (without aggregation and with aggregation). As the surface extends more rapidly, the fluid particles experience less drag and flow resistance in the y direction. This occurs because the surface is stretching more quickly. This is particularly important in the y-direction because the stretching action acts to pull the fluid away from the surface in this direction. Additionally, the presence of nanoparticles in the nanofluid can boost the lubricating effect that is produced near the surface that is being stretched. As the volume fraction rises, there will be a greater number of nanoparticles present between the surface and fluid. This will result in a reduction in frictional forces and contribute to a reduction in the skin friction in y-direction.

Fig. 25 presents $Re_x^{-1/2}Nu_x$ is the function of volume fraction φ for $TiO_2 - C_2H_6O_2$ against different values of rotation variable λ. For greater values of rotation variable and higher wall thickness there is an increment in $Re_x^{-1/2}Nu_x$. The rotation of the surface can bring about changes in the features of the boundary layer. When rotational flows are present, the boundary layer tends to thin out, which results in lower thermal resistance close to the surface. Heat may be transferred more effectively, and thermal energy can be dissipated into the fluid at a faster rate when there is a thinner boundary layer. Incorporating nanoparticles into the system can also modify the thermal characteristics of the nanofluid. Because of the increased density of the nanoparticle suspension, the total thermal conductivity of nanofluid is improved as the volume fraction of the nanofluid increases. Because of the higher thermal conductivity, heat is transferred more effectively, which contributes to an increased Nusselt number. Figs. 26 and 27 shows that the variations in Nusselt number because of the values of Rd and θ_w rise. The convective heat transfer from surface to the fluid can be characterized using a quantity known as the Nusselt number, which is an unmeasured quantity. The importance of radiative heat transmission in the system grows in proportion to the degree to which the radiation parameter is increased. Radiative heat transfer is a process that does not require any physical contact between the surface and the fluid. Instead, it enables the transmission of direct energy with electromagnetic waves. The higher the volume percentage, the higher the concentration of nanoparticles that are present in the nanofluid, which ultimately results in the nanofluid having a greater capacity to absorb radiation. This indicates that the nanofluid can absorb a greater amount of heat radiation coming from the surface. If the radiation parameter is increased, then a greater amount of heat will be transported through radiation from the surface to the nanofluid. This will result in an increase in the Nusselt number. Due to increase in temperature ratio parameter θ_w, the Nusselt number increased for stretched sheets, as seen in Fig. 27. With an increase in the temperature ratio parameter, the temperature difference between the surface and the nanofluid will also rises. As a result of this increased temperature difference between the surface and the fluid, the convective heat transfer from the surface to the fluid is augmented, leading to higher heat transfer rates. The overall thermal conductivity of the nanofluid has been demonstrated to increase

Table 3
Table: Skin friction and Nusselt number at different nanoparticle volume fractions when $\theta_r = -0.5, M = Rd = \theta_w = \lambda = \alpha = 0$ and $Pr = 204$ for aggregation model.

φ	Skin friction in x direction	$Re_{y^{1/2}}Cf_y$	Nusselt number
0.01	− 2.68739	1.1165	1.69275
0.02	− 3.18201	1.25741	1.65668
0.03	− 3.54873	1.43054	1.62487
0.04	− 3.96981	1.64723	1.59718

proportionally with an increase in the volume fraction. Due to its improved thermal conductivity, the nanofluid can more efficiently transfer heat to the surrounding fluid, leading to a higher Nusselt number.

4.4. Table discussion

Table 3 displays the values of skin friction and the Nusselt number that were determined from the current model for potential usage in the future. Shear stress $f''(0)$ is compared by using Table 4 to previous research [24] of viscous fluid. The current findings are consistent with previous research under certain conditions. This demonstrates the present results' validity as well as the accuracy of numerical approach used in this study. Numerical values of several physical parameters of $TiO_2 - C_2H_6O_2$ nanofluid for local Nusselt number with aggregation effects can be found in Table 5. This table also provides comparison for three situations. For rotating flow, radiation types: linear radiation, non-linear radiation, and no radiation. Under any condition radiation accelerates heat transfer. The Nusselt number becomes lower in presence of no radiation impact. Nonlinear radiation has highest heat transmission rate among all types.

5. Conclusion

This study is made because there are a variety of applications for MHD bidirectional rotating flow in engineering and industry, and one of those applications is being investigated here. However, it also possesses a great deal of unknown behaviours and characteristics of its body that have not yet been thoroughly researched. Therefore, the purpose of this study is to investigate how the magnetic parameter, the stretching, the volume fraction, the variable viscosity, the rotation, and the MHD bidirectional rotating flow over the stretching sheet affect the behavior of heat transfer, velocity profile skin friction, and temperature profile. This study presents numerical investigation of heat transfer on MHD bidirectional rotating flow of $TiO_2 - C_2H_6O_2$ nanofluid over a stretching surface in three dimensions. Here is a summary of the findings from the present study:

- The velocity profile is lower due to the aggregation effects. This shows that velocity profile turns to be lowered than that obtained using conventional homogeneous models.
- Nusselt number profiles are higher for aggregation effects model because clustering of nanoparticles in the nanofluid can enhance its effective thermal conductivity.
- The velocity profiles $f'(\eta)$ and $g'(\eta)$ upsurges with increasing values of φ, θ_r because of this decrease in viscous dissipation, less energy is turned into heat because of the friction that occurs inside the fluid, which ultimately results in lower temperatures within the nanofluid.
- As the volume fraction φ of nanoparticles in the nanofluid increases, the temperature profile rises due to the concurrent increase in the overall thermal conductivity of the nanofluid. This increase in thermal conductivity can result in increased heat transfer rates ..
- Skin friction profiles in both directions shows positive behavior with θ_r due to high thermal conductivity and M due to Lorentz forces against φ whereas negative trends show for λ and α..
- Nonlinear radiation Rd, variable viscosity θ_r, rotation λ and temperature ratio, θ_w parameters results increase local Nusselt number.
- When a 1 % volume fraction of nanoparticles is introduced, the Nusselt number exhibits a 0.174 % increase for the aggregation model compared to the regular fluid in the absence of radiation effects.
- In the context of the nonlinear radiation case, the application of a 1 % volume fraction results in a 0.68 % increase in the Nusselt number compared to the regular fluid.
- In the case of linear radiation, when a 1 % volume fraction is introduced, the Nusselt number exhibits a 1.007 % increase compared to the regular fluid.
- When the aggregation model is used with a 1 % volume fraction of nanoparticles, the skin friction increases by 0.1153 % in the x direction and by 0.1165 % in the y direction compared to the regular fluid.

This research fills a void in the existing literature by investigating the effects of novel concepts such as thermal radiation, variable viscosity, and nanoparticle aggregation on the flow of MHD nanofluids over stretched surfaces in three dimensions. In terms of the physical effects, there is an increase in the rate of heat transfer because of the impacts of nanoparticle aggregation, viscosity, and nonlinear thermal radiation. It can be stated that increasing heat transmission via the effects of thermal radiation, viscosity, and nanoparticle aggregation has far-reaching implications in a variety of sectors, ranging from energy efficiency and industrial processes to environmental applications. These implications are expected to have a significant impact on the future of these fields. Research needs to be continued in this field if we are going to be able to come up with new and novel methods of heat transmission and find solutions to the pressing global problems associated with energy and climate change.

Table 4

$f''(0), \varphi = \varphi_a = \theta_r = M = Rd = \theta_w = 0, \alpha = 1$ and $Pr = 6.2$ gives result for specific values of λ.

λ	Current Outcomes	Y. Y. Teh and A. Asghar [24]
0	-1.0	-1.0
0.5	-1.13838	-1.138374
1.0	-1.32503	-1.325029

Table 5
Nusselt number values for different situations of $TiO_2 - C_2H_6O_2$ due to aggregation effects. For $M = 0.5$..

φ_a	θ_r	λ	α	Rd	No Radiation	Linear Radiation $\theta_w = 1.0$	Nonlinear Radiation $\theta_w = 0.4$
0.012	—	0.2	0.5	0.5	2.03508	6.32193	28.7152
	0.5						
0.024	—	—			1.98314	6.35897	28.879
0.036	—	—			1.93923	6.40807	29.0764
0.047	—	—			1.90588	6.46369	29.2868
0.024	—	—			1.98314	6.35897	28.879
	0.5						
—	—	—			2.07608	6.56738	29.4145
	1.0						
—	—	—			2.11237	6.6473	29.6097
	1.5						
—	—	—			2.13179	6.68966	29.7108
	2.0						
—		0.2			1.98314	6.408	29.0061
—	—	0.3			1.9513	6.35897	28.879
—	—	0.5			1.8822	6.29862	28.7242
—	—	0.6			1.84798	6.233	28.5541
			0.5		1.98314	6.35897	28.879
			1.0		2.34388	7.45339	33.655
			1.5		2.64124	8.37434	37.738
			2.0		2.90183	9.18927	41.3778
				0.5		4.76923	28.0105
				0.9		4.28188	20.728
				1.4		4.12063	16.593
				2.0		4.08748	13.9235

Ethical approval

Not applicable.

Data availability

"Data will be made available on request".

CRediT authorship contribution statement

Aisha M. Alqahtani: Validation, Visualization, Writing – review & editing. **Khadija Rafique:** Conceptualization, Formal analysis, Investigation, Methodology, Validation, Writing – original draft. **Zafar Mahmood:** Conceptualization, Data curation, Formal analysis, Supervision. **Bushra R. Al-Sinan:** Data curation, Software, Writing – review & editing. **Umar Khan:** Conceptualization, Investigation, Methodology, Resources, Supervision, Validation. **Ahmed M. Hassan:** Data curation, Investigation, Software, Visualization, Writing – review & editing.

Declaration of competing interest

The authors declare that they have no known competing financial interests or personal relationships that could have appeared to influence the work reported in this paper.

Acknowledgments

References

[1] S. Jana, A. Salehi-Khojin, W.-H. Zhong, Enhancement of fluid thermal conductivity by the addition of single and hybrid nano-additives, Thermochim. Acta 462 (1) (Oct. 2007) 45–55, https://doi.org/10.1016/j.tca.2007.06.009.

[2] S.U.S. Choi, Z.G. Zhang, W. Yu, F.E. Lockwood, E.A. Grulke, Anomalous thermal conductivity enhancement in nanotube suspensions, Appl. Phys. Lett. 79 (14) (Oct. 2001) 2252–2254, https://doi.org/10.1063/1.1408272.

[3] Y. Xuan, Q. Li, Heat transfer enhancement of nano¯uids 7 (2000).

[4] A. Akbarinia, M. Abdolzadeh, R. Laur, Critical investigation of heat transfer enhancement using nanofluids in microchannels with slip and non-slip flow regimes, Appl. Therm. Eng. 31 (4) (Mar. 2011) 556–565, https://doi.org/10.1016/j.applthermaleng.2010.10.017.

[5] A.J. Chamkha, M. Molana, A. Rahnama, F. Ghadami, On the nanofluids applications in microchannels: a comprehensive review, Powder Technol. 332 (Jun. 2018) 287–322, https://doi.org/10.1016/j.powtec.2018.03.044.

[6] P.M. Patil, S. Roy, E. Momoniat, Thermal diffusion and diffusion-thermo effects on mixed convection from an exponentially impermeable stretching surface, Int. J. Heat Mass Tran. 100 (Sep. 2016) 482–489, https://doi.org/10.1016/j.ijheatmasstransfer.2016.04.054.

[7] P.M. Patil, A. Shashikant, S. Roy, E. Momoniat, Unsteady mixed convection over an exponentially decreasing external flow velocity, Int. J. Heat Mass Tran. 111 (Aug. 2017) 643–650, https://doi.org/10.1016/j.ijheatmasstransfer.2017.04.016.

[8] A. Zeeshan, R. Ellahi, F. Mabood, F. Hussain, Numerical study on bi-phase coupled stress fluid in the presence of Hafnium and metallic nanoparticles over an inclined plane, Int. J. Numer. Methods Heat Fluid Flow 29 (8) (Jan. 2019) 2854–2869, https://doi.org/10.1108/HFF-11-2018-0677.

[9] G.S. Seth, M.K. Mishra, Analysis of transient flow of MHD nanofluid past a non-linear stretching sheet considering Navier's slip boundary condition, Adv. Powder Technol. 28 (2) (Feb. 2017) 375–384, https://doi.org/10.1016/j.apt.2016.10.008.

[10] N.K. Mishra, Adnan, G. Sarfraz, M.Z. Bani-Fwaz, S.M. Eldin, Dynamics of Corcione nanoliquid on a convectively radiated surface using Al2O3 nanoparticles, J. Therm. Anal. Calorim. (1–12) (2023).

[11] S.C. Reddy, K.K. Asogwa, M.F. Yassen, Z. Iqbal, B. Ali, S. Km, Dynamics of MHD second-grade nanofluid flow with activation energy across a curved stretching surface, Front. Energy Res. 10 (2022), 1007159.

[12] Z. Mahmood, M. Abd El-Rahman, U. Khan, A.M. Hassan, H.A.E.-W. Khalifa, Entropy generation due to nanofluid flow in porous media over radiative permeable exponentially surface with nanoparticle aggregation effect, Tribol. Int. 188 (2023), 108852.

[13] K. Rafique, Z. Mahmood, U. Khan, Mathematical analysis of MHD hybrid nanofluid flow with variable viscosity and slip conditions over a stretching surface, Mater. Today Commun. 36 (2023), 106692.

[14] M. Abd El-Aziz, Radiation effect on the flow and heat transfer over an unsteady stretching sheet, Int. Commun. Heat Mass Tran. 36 (5) (May 2009) 521–524, https://doi.org/10.1016/j.icheatmasstransfer.2009.01.016.

[15] S. Mukhopadhyay, Effect of thermal radiation on unsteady mixed convection flow and heat transfer over a porous stretching surface in porous medium, Int. J. Heat Mass Tran. 52 (13) (Jun. 2009) 3261–3265, https://doi.org/10.1016/j.ijheatmasstransfer.2008.12.029.

[16] S. Shateyi, S.S. Motsa, Thermal radiation effects on heat and mass transfer over an unsteady stretching surface, Math. Probl Eng. 2009 (Jan. 2010), e965603, https://doi.org/10.1155/2009/965603.

[17] A.H. Ganie, Z. Mahmood, M.M. AlBaidani, N.S. Alharthi, U. Khan, Unsteady non-axisymmetric MHD Homann stagnation point flow of CNTs-suspended nanofluid over convective surface with radiation using Yamada–Ota model, Int. J. Mod. Phys. B (2023), 2350320.

[18] U. Yashkun, K. Zaimi, A. Ishak, I. Pop, R. Sidaoui, Hybrid nanofluid flow through an exponentially stretching/shrinking sheet with mixed convection and Joule heating, Int. J. Numer. Methods Heat Fluid Flow 31 (6) (Jan. 2020) 1930–1950, https://doi.org/10.1108/HFF-07-2020-0423.

[19] S.P.A. Devi, S.S.U. Devi, Numerical investigation of hydromagnetic hybrid Cu – Al2O3/water nanofluid flow over a permeable stretching sheet with suction, Int. J. Nonlinear Sci. Numer. Stimul. 17 (5) (Aug. 2016) 249–257, https://doi.org/10.1515/ijnsns-2016-0037.

[20] S.S.U. Devi, S.P.A. Devi, Numerical investigation of three-dimensional hybrid Cu–Al2O3/water nanofluid flow over a stretching sheet with effecting Lorentz force subject to Newtonian heating, Can. J. Phys. 94 (5) (May 2016) 490–496, https://doi.org/10.1139/cjp-2015-0799.

[21] B. Ali, S. Jubair, D. Fathima, A. Akhter, K. Rafique, Z. Mahmood, MHD flow of nanofluid over moving slender needle with nanoparticles aggregation and viscous dissipation effects, Sci. Prog. 106 (May 2023), 368504231176151, https://doi.org/10.1177/00368504231176151.

[22] I. Waini, A. Ishak, I. Pop, Hybrid nanofluid flow induced by an exponentially shrinking sheet, Chin. J. Phys. 68 (Dec. 2020) 468–482, https://doi.org/10.1016/j.cjph.2019.12.015.

[23] T. Hayat, S. Nadeem, Heat transfer enhancement with Ag–CuO/water hybrid nanofluid, Results Phys. 7 (Jan. 2017) 2317–2324, https://doi.org/10.1016/j.rinp.2017.06.034.

[24] Yuan Ying Teh and Adnan Ashgar, Three dimensional MHD hybrid nanofluid flow with rotating stretching/shrinking sheet and joule heating, CFD Lett. 13 (8) (Aug. 2021) 1–19, https://doi.org/10.37934/cfdl.13.8.119.

[25] P.M. Patil, B. Goudar, Impact of impulsive motion on the Eyring-Powell nanofluid flow across a rotating sphere in MHD convective regime: entropy analysis, J. Magn. Magn Mater. 571 (Apr. 2023), 170590, https://doi.org/10.1016/j.jmmm.2023.170590.

[26] P.M. Patil, S. Benawadi, B. Shanker, Influence of mixed convection nanofluid flow over a rotating sphere in the presence of diffusion of liquid hydrogen and ammonia, Math. Comput. Simulat. 194 (Apr. 2022) 764–781, https://doi.org/10.1016/j.matcom.2021.12.022.

[27] B.M. Makhdoum, Z. Mahmood, U. Khan, B.M. Fadhl, I. Khan, S.M. Eldin, Impact of suction with nanoparticles aggregation and joule heating on unsteady MHD stagnation point flow of nanofluids over horizontal cylinder, Heliyon 9 (4) (2023).

[28] K. Rafique, et al., Impacts of thermal radiation with nanoparticle aggregation and variable viscosity on unsteady bidirectional rotating stagnation point flow of nanofluid, Mater. Today Commun. 36 (2023), 106735.

[29] H.A. Otman, Z. Mahmood, U. Khan, S.M. Eldin, B.M. Fadhl, B.M. Makhdoum, Mathematical Analysis of Mixed Convective Stagnation Point Flow over Extendable Porous Riga Plate with Aggregation and Joule Heating Effects, Heliyon, 2023.

[30] K.A.M. Alharbi, M.Z. Bani-Fwaz, S.M. Eldin, M.F. Yassen, Numerical heat performance of TiO2/Glycerin under nanoparticles aggregation and nonlinear radiative heat flux in dilating/squeezing channel, Case Stud. Therm. Eng. 41 (2023), 102568.

[31] Y. He, Y. Jin, H. Chen, Y. Ding, D. Cang, H. Lu, Heat transfer and flow behaviour of aqueous suspensions of TiO2 nanoparticles (nanofluids) flowing upward through a vertical pipe, Int. J. Heat Mass Tran. 50 (11) (Jun. 2007) 2272–2281, https://doi.org/10.1016/j.ijheatmasstransfer.2006.10.024.

[32] R. Ellahi, M. Hassan, A. Zeeshan, Aggregation effects on water base Al2O3—nanofluid over permeable wedge in mixed convection, Asia Pac. J. Chem. Eng. 11 (2) (2016) 179–186, https://doi.org/10.1002/apj.1954.

[33] J. Mackolil, B. Mahanthesh, Sensitivity analysis of Marangoni convection in TiO2–EG nanoliquid with nanoparticle aggregation and temperature-dependent surface tension, J. Therm. Anal. Calorim. 143 (3) (Feb. 2021) 2085–2098, https://doi.org/10.1007/s10973-020-09642-7.

[34] B. Makhdoum, Z. Mahmood, B. Fadhl, M. Aldhabani, U. Khan, S. Eldin, Significance of entropy generation and nanoparticle aggregation on stagnation point flow of nanofluid over stretching sheet with inclined Lorentz force, Arab. J. Chem. 16 (Mar. 2023), 104787, https://doi.org/10.1016/j.arabjc.2023.104787.

[35] Y. Xuan, Q. Li, W. Hu, Aggregation structure and thermal conductivity of nanofluids, AIChE J. 49 (4) (2003) 1038–1043, https://doi.org/10.1002/aic.690490420.

[36] Z. Mahmood, U. Khan, Nanoparticles aggregation effects on unsteady stagnation point flow of hydrogen oxide-based nanofluids, Eur. Phys. J. Plus 137 (6) (Jun. 2022) 750, https://doi.org/10.1140/epjp/s13360-022-02917-y.

[37] Z. Mahmood, U. Khan, Numerical investigation of nanoparticle aggregation and heat transfer on mixed convective stagnation point flow of nanofluid over extendable vertical Riga plate, Phys. Scripta 98 (Jun) (2023), https://doi.org/10.1088/1402-4896/acd91f.

[38] A.C. Eringen, Theory of thermomicrofluids, J. Math. Anal. Appl. 38 (2) (May 1972) 480–496, https://doi.org/10.1016/0022-247X(72)90106-0.

[39] A.M. Salem, Variable viscosity and thermal conductivity effects on MHD flow and heat transfer in viscoelastic fluid over a stretching sheet, Phys. Lett. 369 (4) (Sep. 2007) 315–322, https://doi.org/10.1016/j.physleta.2007.04.104.

[40] M.A. Seddeek, F.A. Salama, The effects of temperature dependent viscosity and thermal conductivity on unsteady MHD convective heat transfer past a semi-infinite vertical porous moving plate with variable suction, Comput. Mater. Sci. 40 (2) (Aug. 2007) 186–192, https://doi.org/10.1016/j.commatsci.2006.11.012.

[41] S. Mukhopadhyay, G.C. Layek, Sk A. Samad, Study of MHD boundary layer flow over a heated stretching sheet with variable viscosity, Int. J. Heat Mass Tran. 48 (21) (Oct. 2005) 4460–4466, https://doi.org/10.1016/j.ijheatmasstransfer.2005.05.027.

[42] K. Rafique, et al., Investigation of thermal stratification with velocity slip and variable viscosity on MHD flow of Al2O3- Cu- TiO2/H2O nanofluid over disk, Case Stud. Therm. Eng. 49 (2023), 103292.

[43] K. Rafique, Z. Mahmood, U. Khan, Mathematical analysis of MHD hybrid nanofluid flow with variable viscosity and slip conditions over a stretching surface, Mater. Today Commun. 36 (2023), 106692.

[44] K. Rafique, Z. Mahmood, U. Khan, S.M. Eldin, A.M. Alzubaidi, Mathematical Analysis of Radius and Length of CNTs on Flow of Nanofluid over Surface with Variable Viscosity and Joule Heating, Heliyon, 2023, e17673.